ACS OMEGA

http://pubs.acs.org/journal/acsodf

Article

Simultaneous Sensing of Cd(II), Pb(II), and Cu(II) Using Gold Nanoparticle-Modified APTES-Functionalized Indium Tin Oxide Electrode: Effect of APTES Concentration

Noorhashimah Mohamad Nor, Siti Nasirah Nasrul, Nor Dyana Zakaria, and Khairunisak Abdul Razak*

Cite This: *ACS Omega* 2023, 8, 16587−16599

Read Online

ACCESS | Metrics & More | Article Recommendations | Supporting Information

ABSTRACT: In this work, indium tin oxide (ITO) electrodes were functionalized with varying 3-aminopropyltriethoxysilane (APTES) concentration percentages (0.5, 0.75, 1.0, and 2.0 wt %) to obtain the optimum conditions for the assembly of the as-synthesized gold nanoparticles (AuNPs). The AuNP coverage, wettability, and electrochemical performance of the modified electrodes were evaluated. The AuNP/0.75% APTES-ITO-modified electrode exhibited uniform coverage of AuNPs and high electrochemical performance for the simultaneous detection of Cd(II), Pb(II), and Cu(II) ions. Under the optimum conditions, the AuNP/0.75% APTES-ITO-modified electrode showed a linear detection range of 5−120 ppb and limit of detection of 0.73, 0.90, and 0.49 ppb for the simultaneous detection of Cd(II), Pb(II), and Cu(II) ions, respectively, via square wave anodic stripping voltammetry. The modified electrode demonstrated good anti-interference toward other heavy metal ions, good reproducibility, and suitability for application in environmental sample analysis.

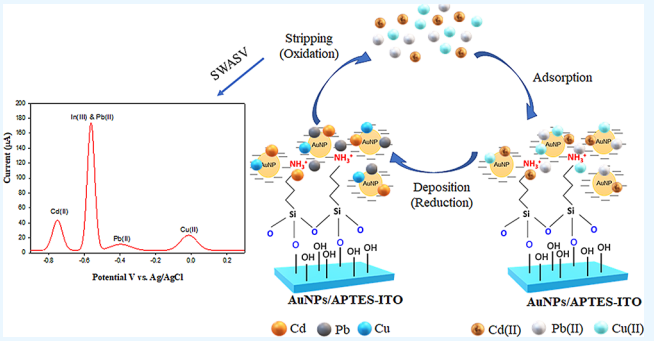

1. INTRODUCTION

Rapid industrialization and urbanization have led to heavy metal pollution becoming a serious problem for the environment and human health. Heavy metals from leaded petrol, industrial effluents, and agricultural activities have been released into the atmosphere, soil, and water.[1] As a result of the nonbiodegradable and toxic nature of heavy metals, they can accumulate in soft tissues and the food chain, posing a serious threat to both health and the environment.[2,3] Therefore, heavy metal concentrations in drinking and industrial wastewaters must be continuously monitored.

In general, spectroscopic techniques such as inductively coupled plasma (ICP)-mass spectrometry, inductively coupled plasma optical emission spectrometry (ICP-OES), and atomic absorption spectrometry have been used in heavy metal detection. These methods have high sensitivity and high selectivity. However, they have drawbacks of expensive equipment and time-consuming sample preparation and cannot be used for on-site measurement. Thus, a sensor for heavy metal detection must be developed. The sensor should be cost-effective, have high accuracy and simple operation, and allow real-time in situ measurements.

Heavy metal sensors include optical sensors, electrochemical sensors, and piezoelectric sensors.[1,4] Electrochemical sensors are favorable for heavy metal detection. These sensors allow the sensitive, selective, inexpensive, and simultaneous detection of heavy metals for on-site monitoring.[1,5] For electrochemical sensors in heavy metal detection, the sensitivity and specificity of the electrochemical sensors are dependent on the working electrode. Conventionally, the working electrode is based on bulk mercury and bismuth. However, these types of electrodes have been replaced because of their toxicity to humans and the environment. Recently, disposable electrodes, such as screen-printed electrodes (SPCEs) and indium tin oxide (ITO) electrodes, have been used for electrochemical heavy metal detection.[6,7]

For electrochemical sensors in heavy metal detection, the anodic stripping voltammetry (ASV) technique is commonly employed because it allows the simultaneous detection of multiple heavy metal ions and features a low limit of detection (LOD).[8] However, the main challenges over simultaneous detection using ASV are the overlapping of peaks due to the close proximity of the potential range between heavy metal ions, competition of the active surface area between heavy metal ions, presence of intermetallic interference, low cathodic

Received: November 3, 2022
Accepted: April 20, 2023
Published: May 5, 2023

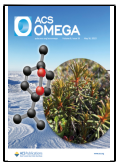

potential limit, and generation of H_2 bubbles during deposition that can cause electrode fouling. To overcome these limitations, a disposable working electrode is commonly modified with nanomaterials and metal film, or chemically modified with polymers and coupling agents.

Chemical modification using conducting polymers such as polyaniline (PANI) and polypyrrole (PPy) or coupling agents like hanethiol hydrochloride, 3-mercaptopropyl trimethoxysilane (MPTMS), and aminopropyltriethoxysilane (APTES) combined with nanoparticles is of interest in the modification of disposable electrodes for heavy metal detection.[9−11] The presence of chemical functional groups, such as amino ($-NH_2$), thiol (−SH), carboxylic (−COOH), alkyl, phenolic, and silane groups, that are able to preconcentrate and absorb heavy metal ions makes the working electrode have high sensitivity and selectivity.[11,12] In addition, the presence of a coupling agent serves as a linker between the surface of the working electrode and nanoparticles to obtain high mechanical stability and robustness of the modified electrode.[13] Meanwhile, the addition of nanoparticles with excellent conductivity, good electrocatalytic activity, and high surface area may further enhance the performance of the modified electrode in heavy metal detection.[14]

Lo et al.[15] developed an aminobenzenediazonium-ITO electrode modified with PPy thin film doped with benzene sulfonic acid modified for the simultaneous detection of Pb(II), Cu(II), and Cd(II) with an LOD of 0.2, 0.7, and 1 ppb, respectively. The presence of a robust PPy film that has good adherence to the aminophenyl-ITO electrode can chelate metal ions and thereby enhance the high sensitivity and selectivity of the modified electrode. Guo et al.[16] reported chemically functionalized silicon nanowires with MPTMS and APTES for the simultaneous detection of Cd(II) and Pb(II) with high sensitivity and specificity and wide linearity of 5−250 nM. The presence of thiol and amino functional groups can form a strong complex with heavy metal ions. Bao et al.[17] developed an SPCE modified layer by layer with the nanocomposite of PANI doped with bismuth nanoparticles, graphene oxide-multiwalled carbon nanotubes (MWCNTs), and chitosan for the simultaneous detection of Hg(II) and Cu(II) with an LOD of 0.1 and 0.03 ppb, respectively.

Currently, many studies have utilized APTES as a coupling agent between the working electrode and nanoparticles for the application of electrochemical sensors. However, most studies utilized APTES-modified electrodes for biosensor applications such as immunosensors,[18] drug delivery,[19] and biomolecule monitoring.[20,21] Kaur et al.[22] have developed bimetallic Au-Pt NPs modified APTES-fluorine tin oxide electrode for electrochemical vitamin D detection, whereas Zhou et al.[21] reported on gold nanoparticles (AuNPs)/electrochemically reduced graphene oxide/APTES-ITO-modified electrode for electrochemical biomolecule monitoring. Most of the published studies on AuNPs and APTES modification were employed for electrochemical biosensor applications.[23,24] There is limited work utilizing APTES and AuNPs for electrode modification in electrochemical heavy metal detection. APTES consists of an amino group with free lone pair electrons on the nitrogen atom to provide suitable sites for effective coupling with heavy metal ions. Alruwais et al.[25] reported on the modification of a glassy carbon electrode (GCE) electrode with a PANI-graphene oxide-APTES composite for Pb(II) detection; their electrode exhibited a linearity of 0.01−0.4 μM and an LOD of 0.0053 μM for Pb(II) detection. Their team then reported[26] on the modification of GCE using PANI, MWCNT, and APTES for Cd(II) detection. The modified electrode of PANI-MWCNT-APTES/GCE showed linearity of detection and an LOD of 0.05−50 and 0.015 μM, respectively. Their studies reported on single heavy metal detection. Recently, they reported on an iron oxide nanoparticle-modified APTES-ITO electrode for the simultaneous detection of Cd(II) and Pb(II)[27] and bismuth nanosheet-modified APTES-SPCE for Pb(II) detection with excellent electrochemical performance.[28]

Inspired by the excellent properties of APTES, in this work, AuNPs assembled with varying concentration percentages on the chemically functionalized APTES-ITO electrode for the simultaneous detection of Cd(II), Pb(II), and Cu(II) were studied. Previously, AuNP-modified electrodes were reported in the simultaneous detection of Cd(II), Pb(II), Hg(II), and Cu(II).[29−31] AuNPs are of interest due to their excellent conductivity, high electrochemical surface area, and catalytic properties, which can enhance electron transfer on the working electrode. Currently, there is lack of published studies that compare the effect of the APTES concentration percentage on the assembly process of AuNPs for the simultaneous detection of heavy metal ions.

The APTES concentration percentage may affect the attachment of organosilane with ITO and the amount of AuNPs assembled and bonded with the $-NH_2$ functional group of APTES that influence the ability of the modified electrode to deposit the heavy metal ions. In this work, the wettability was measured through water contact angle measurements, AuNP coverage was observed via scanning electron microscopy (SEM), and electrochemical performance was analyzed using cyclic voltammetry (CV) and square wave anodic stripping voltammetry (SWASV) analyses. Under the optimized APTES concentration percentage, the modified electrodes' electrochemical performances in terms of linearity, LOD, interference, reproducibility, and real sample analysis were studied in detail for the simultaneous detection of Cd(II), Pb(II), and Cu(II) ions.

2. MATERIALS

All chemicals and reagent used in this work were of analytical grade and used without further purification. Gold(III) chloride trihydrate ($HAuCl_4 \cdot 3H_2O$, ≥99.9%), sodium azide (NaN_3, 99.5%), APTES (99%), potassium ferricyanide ($Fe(CN)_6$, 99%), Pb(II) standard solution, Cd(II) standard solution, Cu(II) standard solution, hydrogen peroxide (H_2O_2, 30 wt %), and sodium acetate buffer solution (HAc-NaAc, pH 5.2) were obtained from Sigma Aldrich. Trisodium citrate dehydrate ($Na_3C_6H_5O_7 \cdot 2H_2O$), hydroxylamine hydrochloride ($NH_2OH \cdot HCl$, 99%), ammonia solution (NH_3, 25%), 2-propanol, ethanol, and potassium chloride (KCl, 99%) were purchased from Merck.

2.1. Apparatus. AuNPs were characterized using Zetasizer (Model ZEN3600, Malvern Instruments, Nano series), X-ray diffraction (XRD; Model D8Advance BRUKER AXS GMBH) with a Cu-Kα radiation source), contact angle goniometer (KSV CAM 101), field-emission scanning electron microscopy (FESEM) with energy dispersive microscopy (Model SUPRA 35VP), and transmission electron spectroscopy (TEM; Model Philips CM12, Version 3.2). Electrochemical measurements were performed using a portable Bipotentiostat/Galvanostat mSTAT 400 (DropSens, Asturias, Spain).

2.2. Synthesis of AuNPs Using the Seeded Growth Method. AuNPs were synthesized using the seeded growth

https://doi.org/10.1021/acsomega.2c07085
ACS Omega 2023, 8, 16587−16599

method as described in our previous work.[32] This method involves two stages, which are Au seed nucleation and the growth of Au seed. In brief, the Au seed was prepared by heating $HAuCl_4 \cdot 3H_2O$ (0.01% w/v) in 125 mL of deionized water to boiling under stirring at 350 rpm. About 2.5 mL of $Na_3C_6H_5O_7 \cdot 2H_2O$ (1% w/v) was added as the reducing agent. At this stage, the color of solution changed from light yellow to faint blue. The solution was kept boiling for 10 min, and the color of solution changed from grayish blue to dark red, indicating the formation of AuNPs. The AuNP seed solution was cooled to room temperature.

The Au seeds were grown to 40 nm of AuNPs. About 16 mL of Au seed solution was diluted in 50 mL of deionized water under stirring at 330 rpm at room temperature. Subsequently, 4 mL of $NH_2OH \cdot HCl$ (0.7% w/v) was added into the Au seed solution. Finally, 2 mL of $HAuCl_4 \cdot 3H_2O$ (1% w/v) was dropwise added into the solution and continuously stirred for 5 min. The AuNPs were collected, and 0.02% w/v of sodium azide (NaN_3) was added. The as-synthesized AuNPs were characterized by XRD to determine the crystallinity and phase. The hydrodynamic size of colloidal AuNPs was analyzed using a Zetasizer, and the particle size was observed by TEM and measured using ImageJ software.

2.3. Self-Assembly of AuNPs on the APTES-Functionalized ITO Electrode. The ITO electrode was cut using a glass cutter and washed with $NH_4OH:H_2O_2:H_2O$ at a ratio of 1:4:20 for 20 min at 60 °C to prepare a hydroxylated active ITO surface. APTES was used as a linker between ITO electrodes and AuNPs. APTES was used to modify the ITO electrodes by surface functionalization for the self-assembly of AuNPs on the surface via the soaking method. APTES was dissolved in absolute ethanol with varying concentrations: 0.5, 0.75, 1, and 2 wt %. The ITO electrodes were immersed in the prepared APTES for 2 h. Subsequently, the ITO electrodes were rinsed thoroughly with ethanol and placed in an oven for 30 min at 100 °C to remove moisture and allow condensation of the silanol (Si−OH) group of APTES with the hydroxyl (−OH) group present on the ITO electrode surface. The APTES-ITO electrode was immersed in AuNPs for 2 h. The AuNP/APTES-ITO-modified electrode was rinsed with distilled water to remove the unbound AuNPs and dried at room temperature. The AuNP/APTES-ITO-modified electrode was characterized by SEM to observe the morphology. Water contact angle measurements were conducted to determine the wettability of the modified electrodes.

2.5. Electrochemical Analysis of Modified Electrodes. CV analysis was conducted to study the electrochemical performance of the modified electrode. CV analysis was performed in 5.0×10^{-3} mol/L potassium ferrocyanide, $(Fe(CN)_6)^{-3/-4}$ containing 0.1 mol/L KCl solution with the scanning range of −0.5 to 0.7 V and scan rate of 50 mV/s. SWASV analysis for simultaneous heavy metal ion detection was conducted in 0.2 M acetate buffer solution. The pH (4.0, 4.5, 5.0, and 5.5), deposition potential (−0.9, −1.0, −1.1, and −1.2 V), and deposition time (120, 180, 240, 300, and 360 s) were varied. SWASV analysis with optimum conditions was conducted with the amplitude of 0.05 V, frequency of 25 Hz, step potential of 0.002 V, and potential scan rage of −1.0 to 0.3 V to evaluate the linearity, LOD, interference, and real sample analysis of the AuNP/APTES-ITO-modified electrodes in the simultaneous detection of Cd(II), Pb(II), and Cu(II).

3. RESULTS AND DISCUSSION

3.1. Characterization of as-Synthesized AuNPs. Figure 1 shows the XRD pattern of the as-synthesized colloidal AuNPs. The as-synthesized colloidal AuNPs were drop casted on a glass slide for XRD analysis. As observed in Figure 1, five diffraction peaks were obtained at (111), (200), (220), and (311) planes, which corresponded to peak positions of 38°, 44°, 65°, and 78°, respectively. The peaks matched with Au with the FCC crystal structure (PDF 98-005-0876). Additionally, NaCl peaks were observed at the (111), (200), (220), and (222) planes with 27°, 31°, and 36°, respectively, which matched with the NaCl pattern of PDF 98-011-6227. The presence of NaCl was observed due to trisodium citrate and gold chloride(III) utilized during the synthesis process.

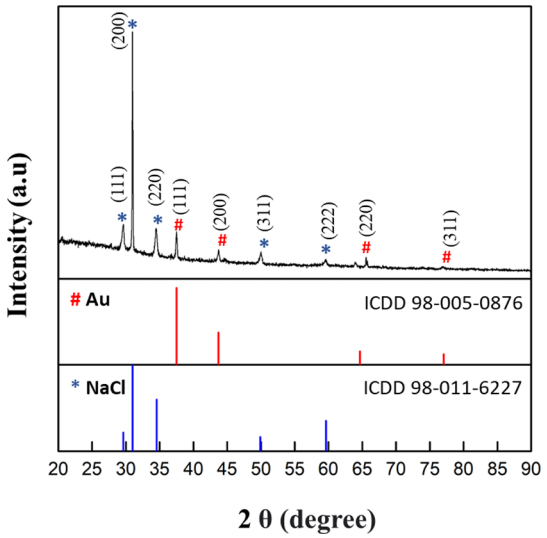

Figure 1. XRD pattern of the as-synthesized colloidal AuNPs.

TEM analysis was conducted to observe the morphology and particle size of the as-synthesized colloidal AuNPs. Figure 2a shows the spherical shape of AuNPs observed from the TEM images. The particle size of AuNPs was analyzed using ImageJ software for 100 particles (Figure 2b), and the results showed that the particle size distribution was in the range of 38−42 nm with mode diameter of 40 nm, which indicated a narrow particle size distribution of the as-synthesized AuNPs. Furthermore, the hydrodynamic particle size measured by dynamic light scattering and polydispersity index of the as-synthesized colloidal AuNPs was quantified using the Zetasizer. The average particle size distribution of AuNPs was 45.55 nm, which was close to the 40 nm particle size measured by TEM analysis. The PDI value of AuNPs was 0.112, which indicated that the AuNP particle size distribution was moderately dispersed in the colloidal suspension.[33]

3.2. Characterization of the Modified Electrodes. The effects of the APTES concentration percentages of 0.5, 0.75, 1.0, and 2.0 wt % on the functionalized ITO electrodes followed by soaking in AuNP solution for 2 h were compared to obtain the optimum concentration percentage of APTES that produced excellent electrochemical performance in heavy metal detection. Water contact angle analysis was performed in this study to analyze the wetting behavior of the modified ITO electrodes. Figures 3 and S1 show the value and cross-sectional image of water contact angles for all modified electrodes. The contact angle value for the unclean bare ITO electrode was

https://doi.org/10.1021/acsomega.2c07085
ACS Omega 2023, 8, 16587−16599

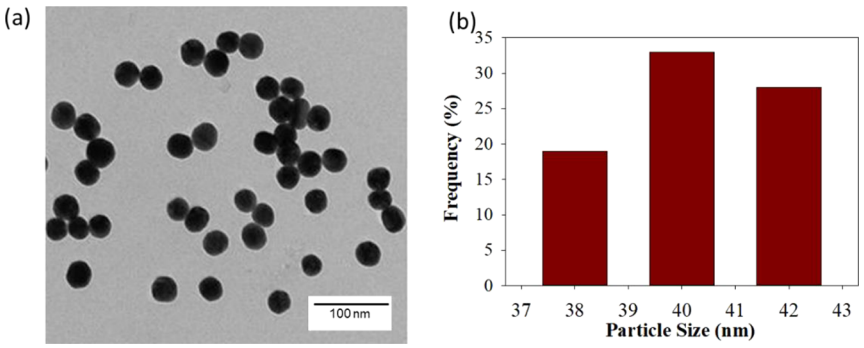

Figure 2. (a) TEM image of the as-synthesized AuNPs and (b) particle size distribution of AuNPs.

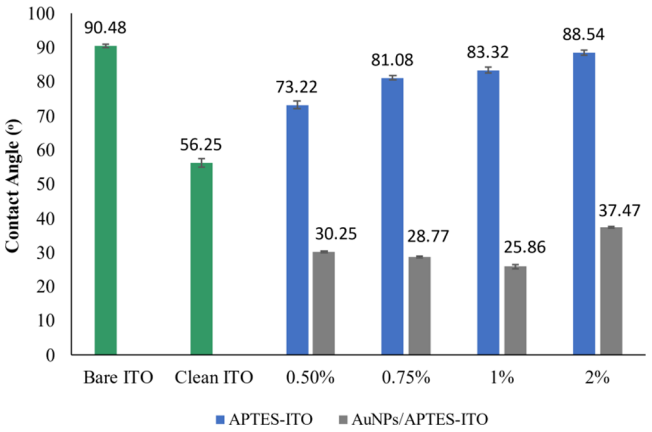

Figure 3. Water contact angles with varying concentration percentages of APTES for the APTES-ITO and AuNP/APTES-ITO electrodes.

90.48°, which indicated hydrophobic properties. After ITO surface treatment with NH_4OH and H_2O_2, the contact angle of bare ITO decreased to 56.25°, which was hydrophilic. The hydrophilic properties were obtained due to the formation of the hydroxyl (−OH) functional group on the surface of the ITO electrode after cleaning. The hydrolyzed surface of the electrode was prepared for further functionalization with APTES.

The mechanism of the APTES-functionalized ITO electrode is shown in Figure 4. APTES consists of three hydrolyzable alkoxy ($-O-CH_2-CH_3$) groups of alkoxysilanes and amine ($-NH_2$) groups at its terminal. During the silanization process, alkoxy hydrolyzed and produced the silanol (Si−O−H) group. The silanol group of APTES subsequently condensed with the hydrolyzed surface of the ITO electrode. Condensation caused the adhesion of APTES on the ITO electrode with the siloxane bond and exposed the $-NH_2$ groups for further binding with AuNPs. Increasing the APTES concentration percentage

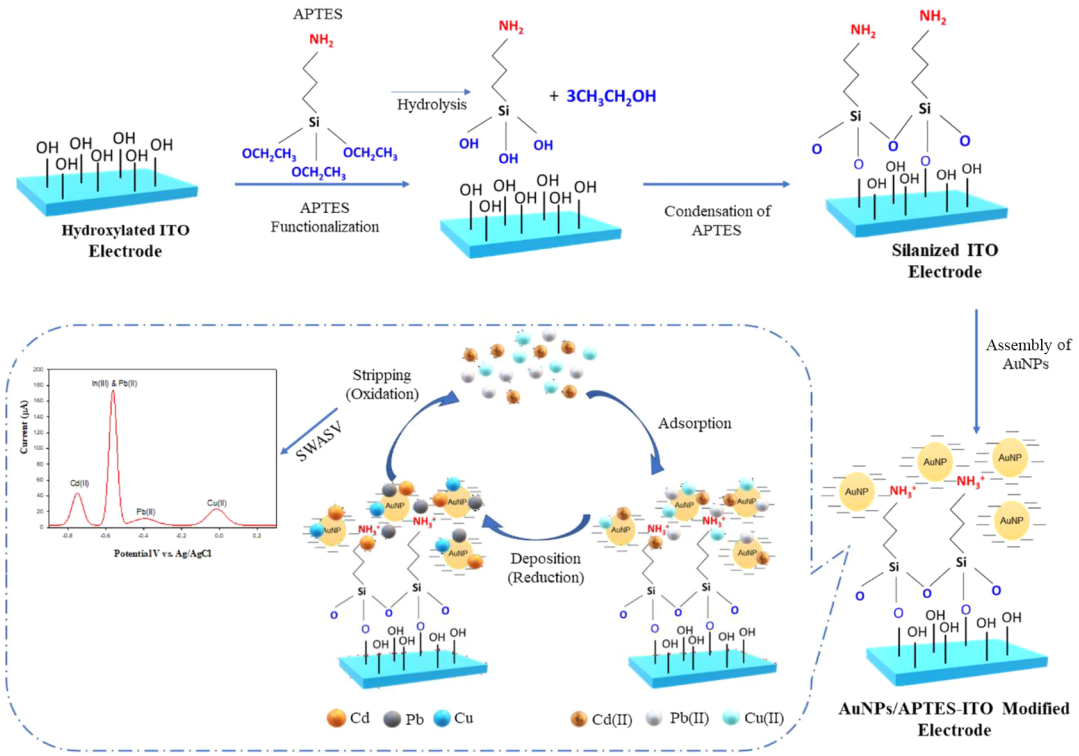

Figure 4. Schematic of silanization of APTES on the ITO electrode, and AuNPs assembled on the APTES-ITO electrode. Inset figure shows the mechanism of simultaneous heavy metal detection of Cd(II), Pb(II), and Cu(II) by the AuNP/APTES-ITO-modified electrode.

https://doi.org/10.1021/acsomega.2c07085
ACS Omega 2023, 8, 16587−16599

increased the presence of alkoxysilanes and amine functional group on the surface of the ITO electrode.

As shown in Figure 3, the contact angles of 73.22°, 81.08°, 83.32°, and 88.54° were obtained for 0.5, 0.75, 1.0, and 2.0 wt % APTES-functionalized ITO electrodes, respectively. The contact angle of the APTES-functionalized electrode was higher and more hydrophobic than that of the clean bare ITO electrode. This result proved the silanization of APTES molecules on the ITO electrode. Increasing the APTES concentration percentage increased the contact angle value of the APTES-modified electrodes, which indicated low wettability. This occurred due to the increase in silanization of APTES on the ITO electrode. With increasing APTES concentration percentage, the condensation of the alkoxy group was expedited, which caused incomplete hydrolysis of silane molecules.[34]

Figure 3 shows that the water contact angles of AuNPs assembled on APTES-ITO with varying APTES concentrations were 30.25°, 28.77°, 25.86°, and 37.47° for 0.5, 0.75, 1.0, and 2.0 wt % APTES concentration, respectively. The water contact angle of the AuNP/APTES-ITO-modified electrode decreased and became more hydrophilic after AuNPs assembled on the APTES-ITO electrode. When immersing the functionalized APTES-ITO in the colloidal AuNP solution, protonation occurred and caused the highly polymerized and unbounded $-NH_2$ group to form NH^{3+}. Subsequently, the negatively charged colloidal AuNPs due to citrate ($-COO^-$) stabilization assembled on NH^{3+} of the APTES-ITO electrode via electrostatic interaction. The assembly of AuNPs on the APTES-ITO-modified electrode decreased the contact angle of the AuNP/APTES-ITO-modified electrode. The contact angle decreased as the percentages of $-COOH$ and $-NH_2$ functional groups increased.[34] However, at 2% of APTES concentration, the water contact angle increased due to the aggregation of AuNPs. At a high APTES concentration percentage, silane polymerized in a random oriented manner which caused aggregation and inhomogeneity of AuNPs assembled on the 2% APTES/ITO-modified electrode. The aggregation reduced the AuNP surface area with negative charge of citrate ($-COO-$) exposed on the modified electrode.

The distribution of AuNPs on APTES-ITO with varying concentration percentages of APTES was observed by FESEM. As shown in Figure 5, the number of AuNPs assembled on APTES-ITO increased with increasing concentration percentage of APTES. Only a low amount of AuNPs assembled on the 0.5% APTES-ITO-modified electrode (Figure 5a). At a low APTES concentration percentage, a longer time was required for the silanization of APTES onto the ITO electrode. Indeed, the silanol group was polymerized in the solvent before reacting with the $-OH$ group on the ITO electrode. Thus, a small amount of $-NH_2$ functional group was present on the 0.5% APTES-ITO-modified electrode for AuNP assembly. Figure 5b shows that more AuNPs assembled on 0.75 wt % APTES-ITO. By increasing the APTES concentration percentage, the silanization interaction was faster than silane polymerization in the solvent, producing a uniform silanization surface. As for 1% APTES-ITO, agglomeration of AuNPs was noted in relation to AuNP assembly (Figure 5c). In the 2% APTES-ITO-modified electrode, aggregation and densely packed assembly of AuNPs on the APTES-ITO electrode were observed (Figure 5d). This phenomenon occurred when the APTES concentration percentage was high, and the silanol

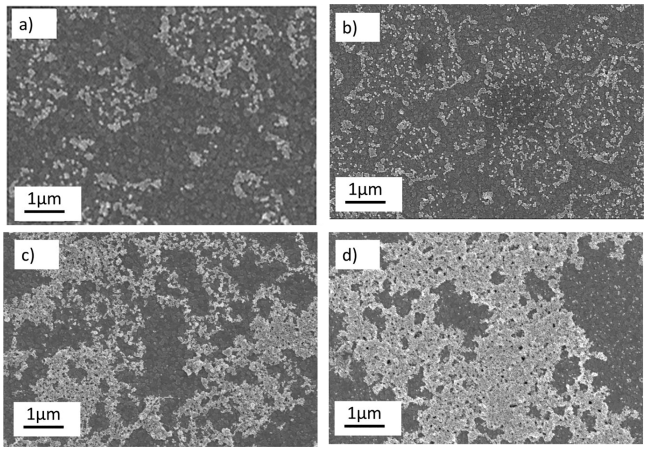

Figure 5. SEM images of AuNPs assembled on (a) 0.5% APTES-ITO-, (b) 0.75% APTES-ITO-, (c) 1.0% APTES-ITO-, and (d) 2% APTES-ITO-modified electrode.

group diffused and reacted with the $-OH$ group but had inadequate time for silane alignment. As a result, silane polymerized in a random oriented manner, which caused the aggregation of AuNPs.

3.3. Electrochemical Characterization of Modified Electrodes. The electrochemical properties of the modified electrodes with varying APTES concentration percentages were studied by CV analysis. Figure 6 and Table 1 show the

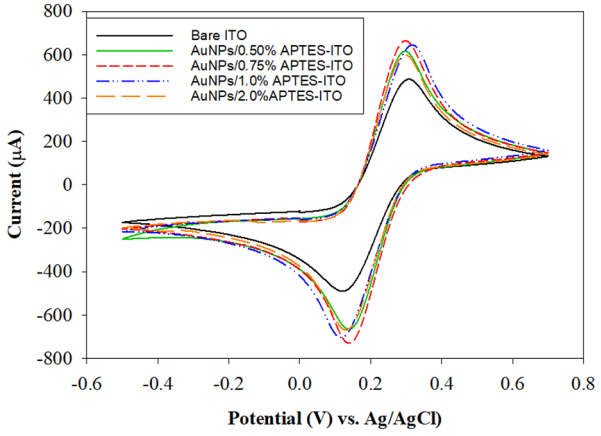

Figure 6. CV analyses of the bare ITO electrode and AuNPs modified with varying APTES concentration percentages on the functionalized ITO electrode in 5.0×10^{-3} mol/L $(Fe(CN)_6)^{-3/-4}$ containing 0.1 mol/L KCl solution with a scan rate of 50 mV/s.

CV curves and summary of the electrochemical performance of bare ITO and AuNP/0.5% APTES-ITO-, AuNP/0.75% APTES-ITO-, AuNP/1.0% APTES-ITO-, and AuNP/2.0% APTES-ITO-modified electrodes examined in 5.0×10^{-3} mol/L $(Fe(CN)_6)^{-3/-4}$ containing 0.1 mol/L KCl solution. Figure 6 shows that the CV peak currents for all modified electrodes increased in both anodic and cathodic peak currents compared with that of the bare ITO electrode. Increase in peak currents values indicates the electrochemical surface area of the modified electrodes for the $[Fe(CN)_6^{3-/4-}]$ redox reaction increased due to the assembly of AuNPs on the APTES-functionalized ITO electrodes. The high conductivity and excellent catalytic properties of AuNPs increase the electrochemical activity of the modified electrodes.

https://doi.org/10.1021/acsomega.2c07085
ACS Omega 2023, 8, 16587−16599

Table 1. Summary of the Electrochemical Performance of Bare ITO and Modified Electrodes

electrode	E_{pa} (V)	E_{pc} (V)	ΔE_p (V)	I_{pa} (μA)	I_{pc} (μA)
bare ITO	0.309	0.121	0.188	493.37	−491.29
AuNPs/0.5% APTES/ITO	0.296	0.140	0.156	641.83	−650.09
AuNPs/0.75% APTES/ITO	0.299	0.140	0.159	692.57	−724.11
AuNPs/1.0% APTES/ITO	0.315	0.115	0.200	660.11	−660.11
AuNPs/2.0% APTES/ITO	0.320	0.115	0.200	659.66	−659.66

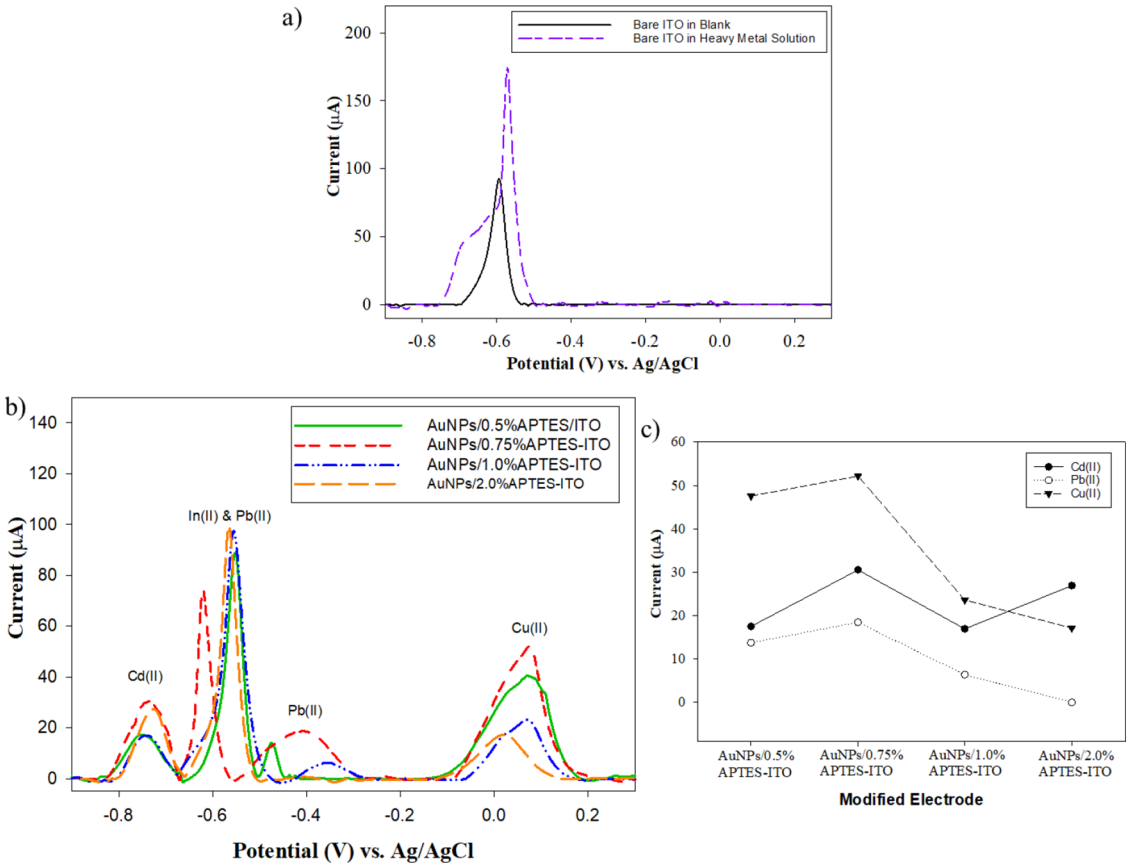

Figure 7. SWASV analysis of (a) bare ITO with and without the presence of 100 ppb Cd(II), Pb(II), and Cu(II); (b) modified electrode for simultaneous heavy metal detection of 100 ppb Cd(II), Pb(II), and Cu(II); (c) stripping peak current of the modified electrode for the simultaneous heavy metal detection of 100 ppb Cd(II), Pb(II), and Cu(II) in 0.2 M acetate buffer solution (pH 4.5).

The bare ITO electrode showed a large peak-to-peak potential difference (ΔE_p) of 0.18 V, whereas ΔE_p for the AuNP/0.5% APTES-ITO- and AuNP/0.75% APTES-ITO-modified electrodes decreased to 0.156 and 0.159 V, respectively. The high conductivity of AuNPs assembled on the APTES-functionalized ITO electrode could enhance the electron transfer rate of redox $Fe(CN)_6^{3-/4-}$ from electrolyte to the working electrode. However, ΔE_p for the AuNP/1.0% APTES-ITO- and AuNP/2.0% APTES-ITO-modified electrodes showed a larger difference (0.200 V) compared with bare ITO. This result was affected by the agglomeration of AuNPs assembled on the 1.0% APTES-ITO electrode and the aggregation of AuNPs assembled on 2.0% APTES-ITO with a densely packed structure as observed in SEM (Figure 5c,d). The aggregation and agglomeration of AuNPs formed a thick film, which reduced the electron transfer rate of redox $Fe(CN)_6^{3-/4-}$ from the electrolyte to the working electrode.

The variation in the APTES concentration percentage influenced the distribution and amount of AuNPs assembled on the APTES-ITO electrode, thereby altering the electrochemical performance of the modified electrode. As shown in Figure 6, the trend of anodic and cathodic peak currents of modified electrodes in descending order was as follows: AuNP/0.75% APTES-ITO > AuNP/1.0% APTES/ITO > AuNP/2.0% APTES/ITO > AuNP/0.5% APTES/ITO > bare ITO. The AuNP/0.75% APTES-ITO electrode showed the highest anodic and cathodic peak currents, which were due to the uniform distribution of AuNPs (Figure 5b). The uniform distribution of AuNPs not only offered the required conduction channel but also functioned as a nanoscale electrode with a larger surface area to encourage the flow of electrons between the electrolyte and the working electrode. By contrast, lower anodic and cathodic peak currents were observed for AuNP/0.5% APTES/ITO due to lesser AuNPs assembled on the APTES-ITO electrode. For the low APTES concentration percentage-functionalized ITO electrode, few $-NH_2$ functional groups were available for AuNPs to assemble, thereby reducing the electrochemical surface area for the $Fe(CN)_6^{3-/4-}$ redox reaction. The AuNP/1.0% APTES/ITO- and AuNP/2.0% APTES/ITO-modified electrodes showed

https://doi.org/10.1021/acsomega.2c07085
ACS Omega 2023, 8, 16587−16599

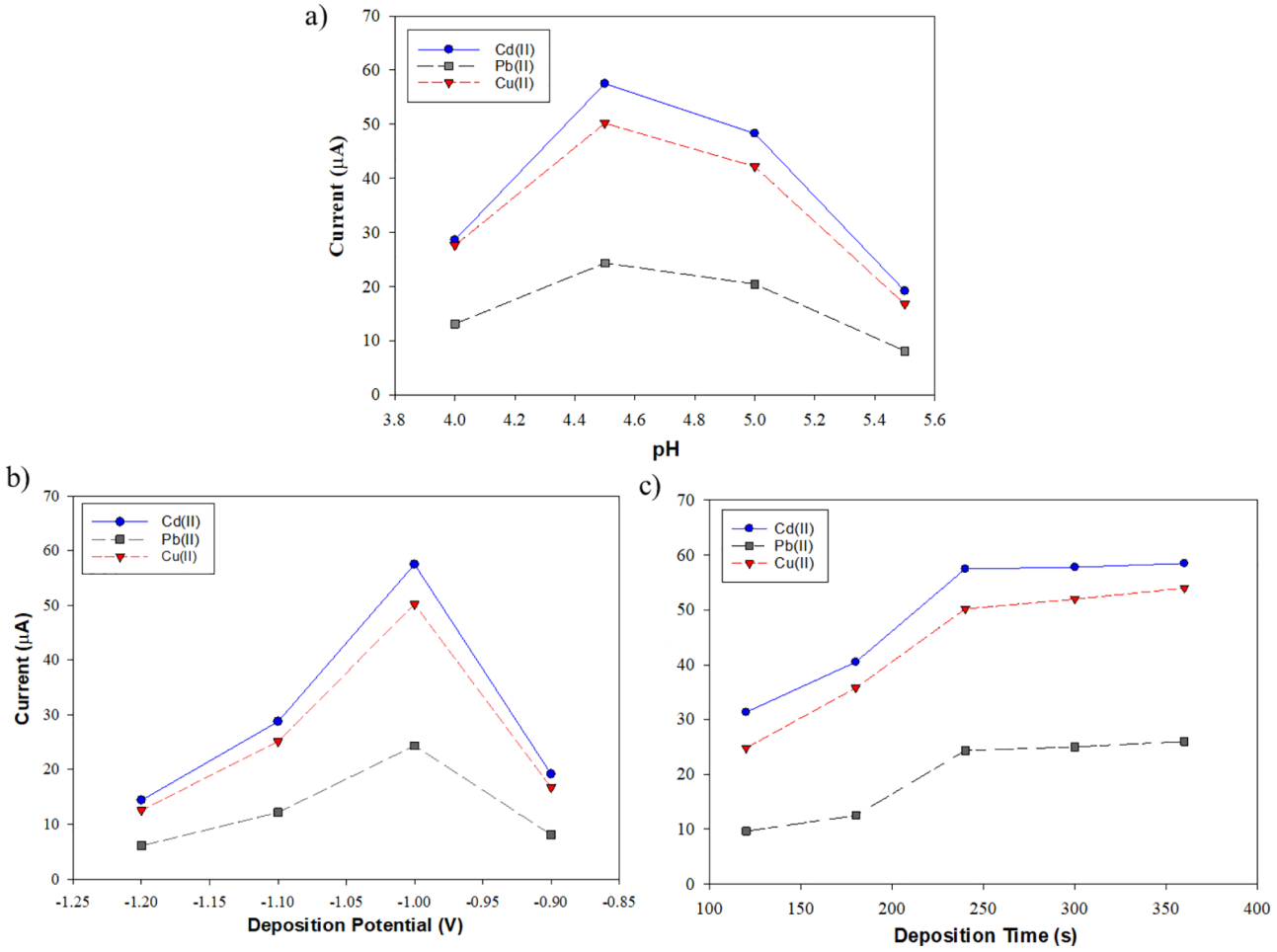

Figure 8. Optimization of SWASV analysis in the simultaneous detection of 100 ppb Cd(II), Pb(II), and Cu(II) as a function of (a) pH, (b) deposition potential, and (c) deposition time in 0.2 M acetate buffer solution.

lower peak current values compared with AuNP/0.75% APTES/ITO. High APTES concentration percentages caused the aggregation of AuNPs on the APTES-ITO electrode, thereby decreasing the electrochemical surface area for the $Fe(CN)_6^{3-/4-}$ redox reaction.

3.4. Electrochemical Properties of the Simultaneous Detection of Cd(II), Pb(II), and Cu(II) on the Modified Electrodes. The electrochemical properties of the bare ITO electrode and modified electrodes for simultaneous heavy metal detection were compared to find the optimum APTES concentration percentage to functionalize ITO electrodes for the assembly of AuNPs. Figure 7a shows the comparison of SWASV analysis for the bare ITO electrode with and without the presence of Cd(II), Pb(II), and Cu(II) ions in 0.2 M acetate buffer solution (pH 4.5). SWASV analysis for the bare ITO without the presence of heavy metal ions (blank solution) showed the stripping peak at −0.58 V with 92.36 μA, which belonged to In(III). A similar observation was reported by other researchers.[35−37] In(III) and Sn(IV) from the ITO electrode were susceptible to oxidation when electrochemical stripping analysis was scanned from more negative potential performed in acidic electrolyte solution. Nonetheless, In(III) was preferred to oxidize against Sn(IV) because of its low oxidation state.[35]

The SWASV analysis of bare ITO in the presence of 100 ppb Cd(II), Pb(II), and Cu(II) ions showed the stripping peak at −0.57 V with 173.44 μA, which belonged to In(III). The current value of the stripping peak of In(III) increased because the In(III) peak position overlapped with Pb(II). Additionally, a shoulder peak coalesced with the In(III) peak at −0.72 V, which may belong to Cd(II). To further confirm this finding, the peak position at −0.57 and −0.58 V belonged to In(III). ICP analysis of the acetate buffer solution containing 100 ppb Cd(II), Pb(II), and Cu(II) ions before and after SWASV analysis was conducted. As listed in Table S1, In(III) ions were not present before SWASV analysis, but 500 ppb of In(III) was detected after SWASV analysis, which revealed that In(III) was etched and oxidized during anodic stripping analysis.

Figure 7b,c shows the SWASV curves and stripping peak current of AuNP/APTES-ITO functionalized with varying APTES concentration percentages for the simultaneous detection of 100 ppb Cd(II), Pb(II), and Cu(II) ions. Among all modified electrodes, AuNP/0.75% APTES-ITO showed the highest anodic stripping peak current value for the simultaneous detection of 100 ppb Cd(II), Pb(II), and Cu(II) ions. This result was attributed to the high amount of AuNPs assembled with uniform distribution on the 0.75%/APTES-ITO-modified electrode. AuNP/0.5% APTES-ITO showed a low stripping peak current due to the low number of AuNPs assembled on the modified electrode. As for AuNP/1.0% APTES-ITO and AuNP/2.0% APTES-ITO, the agglomeration and aggregation of AuNPs reduced the electrochemical surface area for the deposition of heavy metal ions.

https://doi.org/10.1021/acsomega.2c07085
ACS Omega 2023, 8, 16587−16599

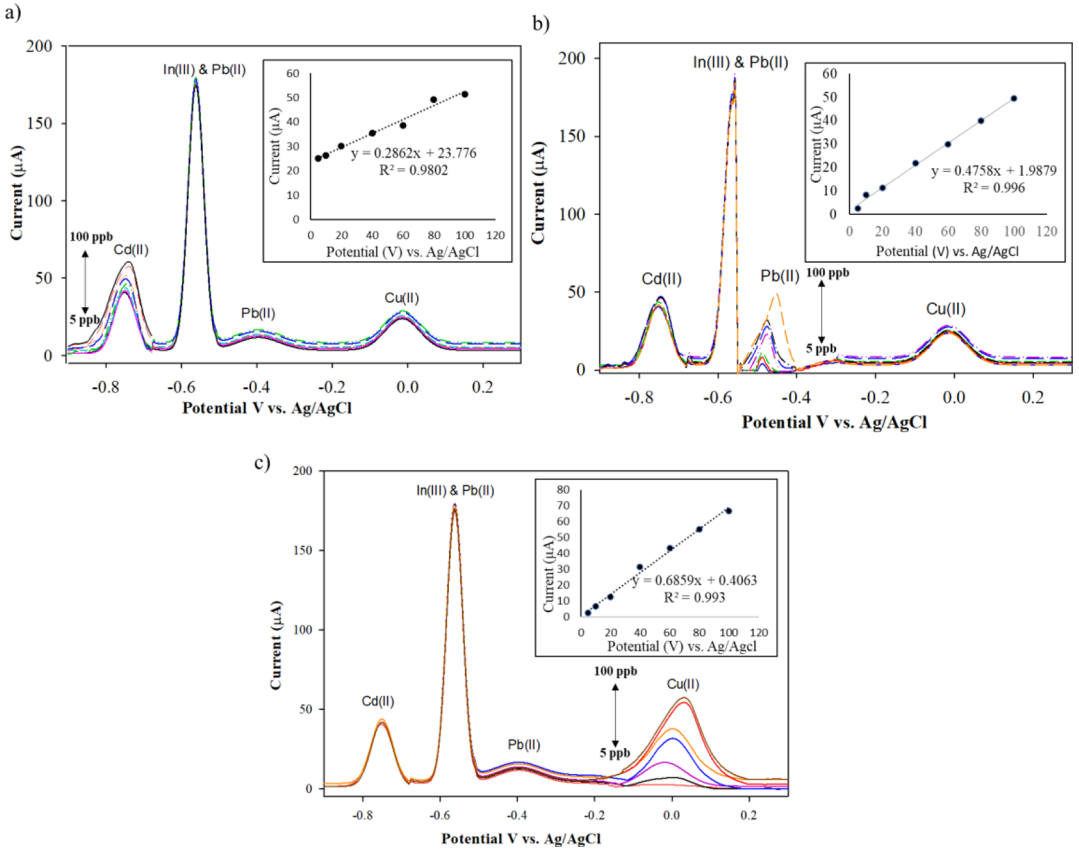

Figure 9. SWASV analysis of AuNP/0.75% APTES-ITO-modified electrodes of (a) Cd(II) ions (5, 10, 20, 40, 60, 80, and 100 ppb) in the presence of 40 ppb Pb(II) and Cu(II) ions, (b) Pb(II) ions (5, 10, 20, 40, 60, 80, and 100 ppb) in the presence of 40 ppb Cd(II) and Cu(II) ions, and (c) Cu(II) ions (5, 10, 20, 40, 60, 80, and 100 ppb) in the presence of 40 ppb Cd(II) and Pb(II) ions evaluated in 0.2 M acetate buffer solution with optimum conditions. Insets are the calibration curves with varying concentration percentages of APTES.

The stripping peak potentials for Cd(II) and Cu(II) ions at −0.74 and −0.09 V were similar for the AuNP/0.5% APTES-ITO-, AuNP/0.75% APTES-ITO-, and AuNP/1.0% APTES-ITO-modified electrodes. The AuNP/2.0% APTES-ITO-modified electrode's Cd(II) peak shifted to a more positive value at −0.72 V. The aggregation of AuNPs assembled on the 2.0% APTES-ITO-modified electrode reduced the electron transfer kinetics. However, the Cu(II) peak for the AuNP/2.0% APTES-ITO-modified electrode shifted to a more negative value because the modified electrode was not able to strip the Pb(II) ions. Instead, the stripping peak of intermetallic Pb-Cu was observed at a more negative value.

The AuNP/0.5% APTES-ITO-modified electrode showed the Pb(II) stripping peak at a more negative position of −0.47 V, which indicated rapid electron transfer. However, given that only a low amount of AuNPs was assembled, the peak current was lower compared with another modified electrode. As for the Pb(II) stripping peak, the peak shifted to more positive values of −0.40 and −0.35 V for the AuNP/0.75% APTES-ITO- and AuNP/1.0% APTES-ITO-modified electrodes, respectively. The electron transfer rate reduced due to the agglomeration of AuNPs on the 1.0% APTES-ITO electrode. As for the AuNP/2.0% APTES-ITO-modified electrode, the Pb(II) peak was not observed due to In(III) and Pb(II) peak coalescence. The aggregation of AuNPs with a dense structure formed a barrier that reduced the electron transfer kinetics. Therefore, the AuNP/0.75% APTES-ITO-modified electrode was the optimum condition electrode for simultaneous heavy metal detection.

3.5. Optimized Performance of Modified Electrodes.

The optimization of parameters including pH of acetate buffer solution, deposition potential, and deposition time for SWASV analysis in the simultaneous detection of Cd(II), Pb(II), and Cu(II) was studied to develop the best electrochemical performance for the AuNP/0.75% APTES-ITO-modified electrode. In SWASV analysis, the pH of the electrolyte buffer solution influences the hydrolysis of metal ions and significantly affects the stripping peak current value in heavy metal detection. In this work, 0.2 M acetate buffer solution varied from pH 4 to pH 5.5 for the simultaneous detection of 100 ppb Cd(II), Pb(II), and Cu(II). As shown in Figure 8a, the highest stripping peak current of Cd(II), Pb(II), and Cu(II) was observed at pH 4.5. The H_2 evolution reaction occurred at pH lower than 4.5. This reaction prevented the deposition of heavy metal ions on the modified electrode and resulted in a low stripping peak current value. High pH forms a metal hydroxide complex, which decreases the metal ion concentration in the electrolyte solution. Thus, a low stripping peak current was obtained. In this work, pH 4.5 was chosen as the optimum condition for subsequent analysis.

The effect of deposition potential of −0.9 to −1.2 V on the stripping peak current response for 100 ppb Cd(II), Pb(II), and Cu(II) ions was evaluated. As shown in Figure 8b, the stripping peak current for Cd(II), Pb(II), and Cu(II) increased with increasing deposition potential from −0.9 to −1.0. At the

https://doi.org/10.1021/acsomega.2c07085
ACS Omega 2023, 8, 16587−16599

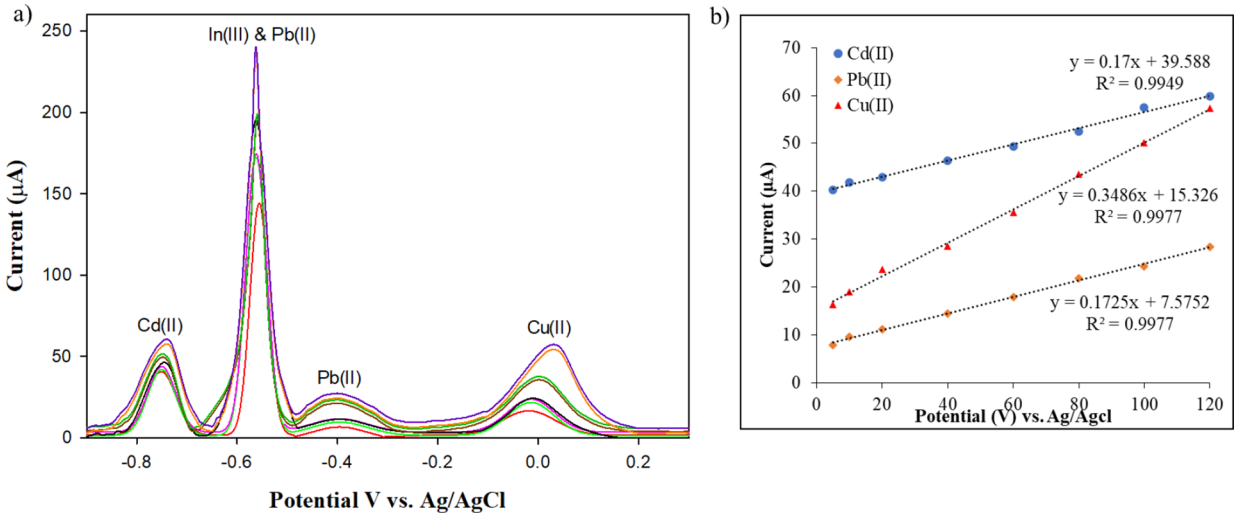

Figure 10. (a) SWASV analysis of the AuNP/0.75% APTES-ITO-modified electrode and (b) calibration curve with varying concentrations of Cd(II), Pb(II), and Cu(II) ions (5, 10, 20, 40, 60, 80, 100, and 120 ppb) evaluated in 0.2 M acetate buffer solution with optimum conditions.

Table 2. Comparison of the Analytical Performance of Various Reported Modified Electrodes with the AuNP/0.75% APTES-ITO-Modified Electrode for the Simultaneous Detection of Heavy Metal Ions

modified electrode	technique/stripping potential	linearity (ppb)	LOD (ppb)	ref
Au nanostar electrodes	Pb(II)	62.3−215.6	20.55	39
	As(III)	10.8−419.4	3.57	
	Hg(II)	33.6−361.5	11.08	
PANI-GO-APTES	Pb(II)	2.0−80.0	1.10	25
IONPs-APTES/ITO	Cd(II)	10.0−100.0	0.90	27
	Pb(II)	10.0−100.0	0.60	
PANI-MWCNT-APTES	Cd(II)	5−5000	1.69	26
AuPtNP/ITO	Hg(II)	0.02−100	0.80	40
Au/PANI/GCE	Pb(II)	4.14−149.18	0.62	31
	Cu(II)	5.00−152.00	0.51	
MPTMS-APTES/Si nanowire/Si	Cd(II)	0.1−28		16
	Pb(II)	1−51		
Au-SPGE	Pb(II)	5−300	2.2	41
	Cu(II)	5−300	1.5	
	Hg(II)	5−300	1.3	
PPy/aminobenzenediazonium-ITO electrode	Cd(II)	11.3−100	1.0	15
	Pb(II)	20.7−51.8	0.2	
	Cu(II)	13.4−100	0.7	
AuNPs/0.75% APTES/ITO	Cd(II)	5−120	1.73	this work
	Pb(II)	5−120	0.90	
	Cu(II)	5−120	0.49	

potential of −1.1 V, the stripping peak current started to decrease. The H_2 evolution reaction occurred at a high negative potential, reducing the deposition of heavy metal ions due to electrode fouling. Therefore, −1.0 V was selected as the optimum deposition potential. As shown in Figure 8c, the effect of deposition time from 120 to 360 s on the stripping peak current response for 100 ppb Cd(II), Pb(II), and Cu(II) ions was evaluated. The stripping peak currents for Cd(II), Pb(II), and Cu(II) increased as the deposition time increased from 120 to 240 s. Only a small increment of the stripping peak's current value was observed when the deposition time further increased from 240 to 360 s. Therefore, the deposition time of 240 s was chosen as the optimum condition for all subsequent studies.

3.6. Analytical Performance of the Modified Electrodes for Simultaneous Detection. The SWASV analysis of the AuNP/0.75% APTES-ITO-modified electrode for the simultaneous detection of Cd(II), Pb(II), and Cu(II) ions was conducted under optimum conditions (pH 4.5, deposition potential of −1.0 V, and deposition time of 240 s) in 0.2 M acetate buffer solution. To observe the effect of mutual interference among the three heavy metal ions (Cd(II), Pb(II), and Cu(II)), SWASV analysis for the simultaneous detection of Cd(II), Pb(II), and Cu(II) was carried out by changing the concentration of one heavy metal ion from 5 ppb to 100 ppb, while fixing the two other heavy metal ions at 40 ppb. Figure 9a−c shows that the stripping peak currents of Cd(II), Pb(II), and Cu(II) increased linearly in the concentration range of 5−100 ppb, with linear equation of $I_p = 0.2862C_{Cd}$ (ppb) + 23.776, $R^2 = 0.9802$; $I_p = 0.4758C_{Pb}$ (ppb) + 1.9879, $R^2 = 0.996$; and $I_p = 0.6859C_{Cu}$ (ppb) + 0.4063, $R^2 = 0.993$, respectively. A high correlation coefficient (R^2) indicated the

https://doi.org/10.1021/acsomega.2c07085
ACS Omega 2023, 8, 16587−16599

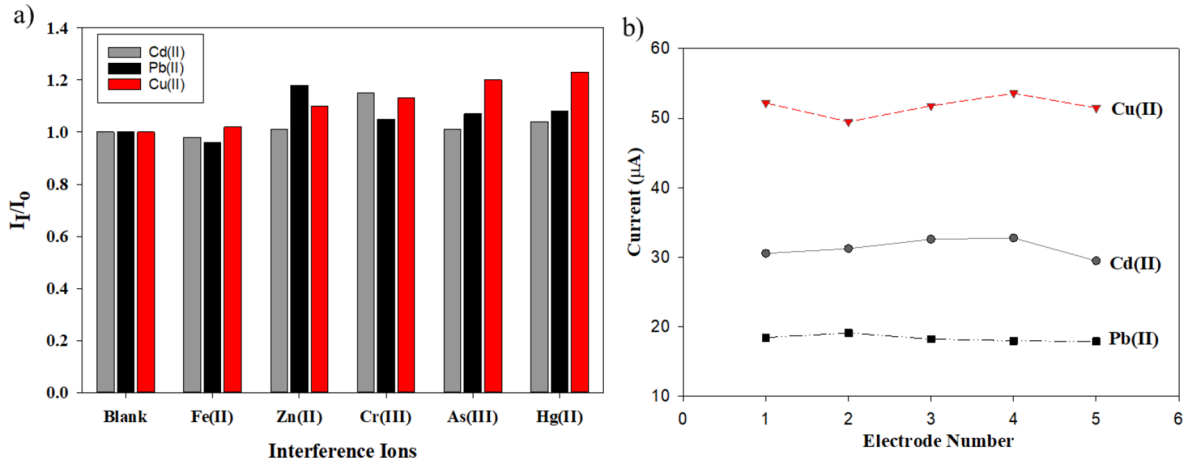

Figure 11. AuNP/0.75% APTES/ITO-modified electrode. (a) Interference stripping peak current ratio (I_I/I_O) in the presence of 40 ppb Cd(II), Pb(II), and Cu(II) ions and 10 times concentration of interference ions of Fe(II), Zn(II), Cr(III), As(III), and Hg(II). (b) Reproducibility for the simultaneous detection of 100 ppb Cd(II) and Pb(II) ions in 0.2 M acetate buffer solution (pH 4.5).

good fitted linear detection of Cd(II), Pb(II), and Cu(II) ions simultaneously in the range of 5−100 ppb. The LODs toward Cd(II), Pb(II), and Cu(II) were 0.65, 0.39, and 0.40 ppb, respectively. The two other fixed concentrations of heavy metal ions showed constant or small changes on the stripping peak current. Thus, the presence of Cd(II), Pb(II), and Cu(II) simultaneously did not interfere with the analytical response of the modified electrodes.

Figure 10 shows the SWASV response of the AuNP/0.75% APTES-ITO-modified electrode in the simultaneous detection of Cd(II), Pb(II), and Cu(II) by increasing the concentration of all three heavy metal ions in the range of 5−120 ppb. The stripping peak currents for Cd(II), Pb(II), and Cu(II) were observed at −0.74, −0.40, and 0.01 V, respectively. Additionally, the stripping peak current of the In(III) and Pb(II) peaks overlapping at −0.55 V was observed. The stripping peak current increased linearly with increasing concentration of Cd(II), Pb(II), and Cu(II). The linear equations of I_p = 0.1700C_{Cd} (ppb) + 39.588, R^2 = 0.9949, and I_p = 0.1725C_{Pb} (ppb) + 7.575, R^2 = 0.9977 I_p = 0.3486C_{Cu} (ppb) + 15.326, R^2 = 0.9765, with an LOD of 1.73, 0.90, and 0.492 ppb were obtained for Cd(II), Pb(II), and Cu(II), respectively. The peak positions, slopes, and calibration curves between individual and simultaneous detection of Cd(II), Pb(II), and Cu(II) did not show large variance. A comparison of the performance of the AuNP/0.75% APTES-ITO-modified electrode in the simultaneous detection of Cd(II), Pb(II), and Cu(II) with other reported studies is listed in Table 2. The LOD of the AuNP/0.75% APTES-ITO-modified electrode in the simultaneous detection of Cd(II), Pb(II), and Cu(II) was comparable with the electrochemical performance reported in previous studies on chemically functionalized electrodes and Au nanomaterial-modified electrodes[15,25,31] but lower than the limit of the World Health Organization for drinking water. The stripping peak potentials for Cd(II), Pb(II), and Cu(II) were distinguished and separated from one another. Thus, this result suggested that the AuNP/0.75% APTES-ITO-modified electrode could simultaneously detect the Cd(II), Pb(II), and Cu(II) ions.

The sensing mechanism of the AuNP/0.75% APTES-ITO-modified electrode in the simultaneous detection of Cd(II), Pb(II), and Cu(II) is illustrated in the inset of Figure 4. The Cd(II), Pb(II) , and Cu(II) ions are adsorbed on the surface of the AuNP/0.75% APTES-ITO-modified electrode via electrostatic interaction of negatively charged AuNPs due to citrate (−COO−) stabilization and via complexation with the $-NH_2$ group of APTES. Then, the heavy metal ions were deposited on zero-valent metals under the potential of −1.0 V for 240 s. During anodic stripping, the zero-valent metals were oxidized and released from the surface of the AuNP/0.75% APTES-ITO-modified electrode. The reaction generates a stripping peak current, which is proportional to the concentration of the heavy metal ions.

The high sensitivity and selectivity of the AuNP/0.75% APTES-ITO-modified electrode toward the simultaneous detection of Cd(II), Pb(II), and Cu(II) is attributed to the high surface area provided by AuNPs for the deposition of heavy metal ions and the high affinity of the $-NH_2$ groups of APTES to form complexation with heavy metal ions. The complexation occurred due to APTES consisting of an amino group with free lone pair electrons on the nitrogen atom that provide suitable sites for effective coupling with heavy metal ions. Moreover, the high electrical conductivity and excellent catalytic properties of AuNPs have facilitated the rapid electron transfer toward oxidation of heavy metals and promoted electrochemical determination, as reported by other researchers.[38]

3.7. Interference and Reproducibility Studies. To evaluate the selectivity and anti-interference ability of the AuNP/0.75% APTES/ITO-modified electrode, the heavy metal ions of As(III), Zn(II), Fe(III), Cr(III), and Mg(II) were added 10 times the concentration of Cd(II), Pb(II), and Cu(II) ions. Figures S2 and 11a show the SWASV peak response, and the ratio of the stripping peak current in the presence of interference ion (I_I) over the stripping peak current without the presence of interference ions (I_o) showed a value close to 1 for all the interference ions, respectively. Thus, the AuNP/0.75% APTES/ITO-modified electrode demonstrated high selectivity for the simultaneous detection of Cd(II), Pb(II), and Cu(II) ions.

The reproducibility of the AuNP/0.75% APTES/ITO-modified electrode was observed by evaluating five different modified electrodes in 0.2 M acetate buffer in the presence of 100 ppb Cd(II), Pb(II), and Cu(II) ions. Figure 11b shows the relative standard deviation of 4.43, 2.16, and 2.86% for Cd(II),

https://doi.org/10.1021/acsomega.2c07085
ACS Omega 2023, 8, 16587−16599

Table 3. Analysis of Seawater Sample without the Addition of Heavy Metal Ions and with the Addition of 10, 30, and 50 ppb Cd(II), Pb(II), and Cu(II) Ions via SWASV Analysis of the AuNP/0.75% APTES-ITO-Modified Electrode and ICP-OES

sample	added (ppb)			SWASV analysis using modified electrode (ppb)			recovery (ppb)			ICP-OES analysis (ppb)		
	Cd(II)	Pb(II)	Cu(II)	Cd(II)	Pb(II)	Cu(II)	Cd(II)	Pb(II)	Cu(II)	Cd(II)	Pb(II)	Cu(II)
seawater Teluk Bahang				ND	1.30					ND	ND	ND
	10.00	10.00	10.00	9.86	11.57	11.43	98.6	102.7	115.7	10.5	11.25	9.42
	30.00	30.00	30.00	30.23	31.56	30.08	100.76	100.86	100.26	31.14	30.05	30.25
	50.00	50.00	50.00	49.87	51.23	49.5	99.74	99.86	99.00	50.25	50.85	49.90

Pb(II), and Cu(II), respectively, indicating the high reproducibility of the AuNP/0.75% APTES/ITO-modified electrode.

3.8. Application in Seawater Sample. The applicability of the AuNP/0.75% APTES/ITO-modified electrode for the simultaneous detection of Cd(II), Pb(II), and Cu(II) ions was assessed in seawater samples under the optimum SWASV condition. The seawater samples from Teluk Bahang were filtered and added with 0.2 M acetate buffer to achieve pH 4.5 prior to SWASV analysis. The SWASV analysis of the seawater samples using the AuNP/0.75% APTES/ITO-modified electrode showed 1.3 ppb Pb(II) ions, whereas Cd(II) and Cu(II) ions were not detected (Table 3). The seawater samples without the addition of heavy metal ions and with the addition of 10, 30, and 50 ppb Cd(II), Pb(II), and Cu(II) heavy metal ions were analyzed by ICP-OES as a comparison. As a result of the detection limit of ICP-OES, the seawater sample without the addition of heavy metal ions was not detected. However, good recoveries were obtained as listed in Table 3 for the seawater sample with the addition of heavy metal ions. This result indicated that the AuNP/0.75% APTES/ITO-modified electrode presented good feasibility for the simultaneous detection of Cd(II), Pb(II), and Cu(II) ions.

4. CONCLUSIONS

In this work, the effect of APTES (0.5, 0.75, 1.0, and 2.0 wt %)-functionalized ITO for the assembly of the as-synthesized AuNPs was evaluated to obtain a high electrochemical performance-modified electrode for the simultaneous detection of Cd(II), Pb(II), and Cu(II) ions. Increasing the APTES concentration percentage increased the assembly of AuNPs because more $-NH_2$ functional groups were available. However, agglomeration and aggregation of AuNPs led to a densely packed structure at high APTES concentrations. The dense distribution of AuNPs reduced the electrochemical performance of the modified electrodes. The AuNP/0.75% APTES-ITO-modified electrode showed the highest electrochemical performance in the simultaneous detection of Cd(II), Pb(II), and Cu(II) ions with an LOD of 1.73, 0.90, and 0.49 ppb, respectively. The modified electrode also showed high anti-interference and feasibility in seawater sample analysis with recovery in the range of 98−115%.

■ ASSOCIATED CONTENT

Supporting Information

The Supporting Information is available free of charge at https://pubs.acs.org/doi/10.1021/acsomega.2c07085.

Cross-sectional image of water contact angles for all modified electrodes and the ICP-OES analysis of 0.2 M acetate buffer solution in the presence of 100 ppb Cd(II), Pb(II), and Cu(II) ions before and after SWASV analysis (PDF)

■ AUTHOR INFORMATION

Corresponding Author

Khairunisak Abdul Razak − *School of Materials and Mineral Resources Engineering, Universiti Sains Malaysia, 14300 Nibong Tebal, Pulau Pinang, Malaysia; NanoBiotechnology Research & Innovation (NanoBRI), INFORMM, Universiti Sains Malaysia, 11800 Gelugor, Pulau Pinang, Malaysia;* orcid.org/0000-0003-0140-2418; Email: khairunisak@usm.my

Authors

Noorhashimah Mohamad Nor − *School of Materials and Mineral Resources Engineering, Universiti Sains Malaysia, 14300 Nibong Tebal, Pulau Pinang, Malaysia;* orcid.org/0000-0001-5692-8287

Siti Nasirah Nasrul − *School of Materials and Mineral Resources Engineering, Universiti Sains Malaysia, 14300 Nibong Tebal, Pulau Pinang, Malaysia*

Nor Dyana Zakaria − *NanoBiotechnology Research & Innovation (NanoBRI), INFORMM, Universiti Sains Malaysia, 11800 Gelugor, Pulau Pinang, Malaysia*

Complete contact information is available at: https://pubs.acs.org/10.1021/acsomega.2c07085

Notes

The authors declare no competing financial interest.

■ ACKNOWLEDGMENTS

The authors acknowledge the financial support from the Universiti Sains Malaysia (Research University Top Down grant 1001/Pbahan/870049).

■ REFERENCES

(1) Hou, H.; Zeinu, K. M.; Gao, S.; Liu, B.; Yang, J.; Hu, J. Recent Advances and Perspective on Design and Synthesis of Electrode Materials for Electrochemical Sensing of Heavy Metals. *Energy Environ. Mater.* **2018**, *1*, 113−131.

(2) Briffa, J.; Sinagra, E.; Blundell, R. Heavy metal pollution in the environment and their toxicological effects on humans. *Heliyon* **2020**, *6*, No. e04691.

(3) Ali, H.; Khan, E.; Ilahi, I. Environmental Chemistry and Ecotoxicology of Hazardous Heavy Metals: Environmental Persistence, Toxicity, and Bioaccumulation. *J. Chem.* **2019**, *2019*, No. 6730305.

(4) Liu, X.; Zhang, Q.; Wu, Z.; Shi, X.; Zhao, N.; Qiao, Y. Rapid Elemental Analysis and Provenance Study of Blumea balsamifera DC Using Laser-Induced Breakdown Spectroscopy. *Sensors* **2015**, *15*, 642−655.

(5) Nguyen, M. B.; Nga, D. T. N.; Thu, V. T.; Piro, B.; Truong, T. N. P.; Yen, P. T. H.; Le, G. H.; Hung, L. Q.; Vu, T. A.; Ha, V. T. T. Novel nanoscale Yb-MOF used as highly efficient electrode for simultaneous detection of heavy metal ions. *J. Mater. Sci.* **2021**, *56*, 8172−8185.

(6) Mohamad Nor, N.; Ramli, N. H.; Poobalan, H.; Qi Tan, K.; Abdul Razak, K. Recent Advancement in Disposable Electrode Modified with Nanomaterials for Electrochemical Heavy Metal Sensors. *Crit. Rev. Anal. Chem.* **2023**, *53*, 253.
(7) Silah, H.; Erkmen, C.; Demir, E.; Uslu, B. Modified indium tin oxide electrodes: Electrochemical applications in pharmaceutical, biological, environmental and food analysis. *TrAC, Trends Anal. Chem.* **2021**, *141*, No. 116289.
(8) Borrill, A. J.; Reily, N. E.; Macpherson, J. V. Addressing the practicalities of anodic stripping voltammetry for heavy metal detection: a tutorial review. *Analyst* **2019**, *144*, 6834−6849.
(9) Mahadik, M.; Patil, H.; Bodkhe, G.; Ingle, N.; Sayyad, P.; Al-Gahaouri, T.; Shirsat, S. M.; Shirsat, M. EDTA Modified PANI/GO Composite Based Detection of Hg (II) Ions. *Front. Mater.* **2020**, *7*, 81.
(10) Eswaran, M.; Tsai, P.-C.; Wu, M.-T.; Ponnusamy, V. K. Novel nano-engineered environmental sensor based on polymelamine/graphitic-carbon nitride nanohybrid material for sensitive and simultaneous monitoring of toxic heavy metals. *J. Hazard. Mater.* **2021**, *418*, No. 126267.
(11) Huang, H.; Wang, Y.; Zhang, Y.; Niu, Z.; Li, X. Amino-functionalized graphene oxide for Cr(VI), Cu(II), Pb(II) and Cd(II) removal from industrial wastewater. *Open Chem.* **2020**, *18*, 97−107.
(12) Kusutaki, T.; Furukawa, M.; Tateishi, I.; Katsumata, H.; Kaneco, S. Preconcentration of Pb with Aminosilanized Fe3O4 Nanopowders in Environmental Water Followed by Electrothermal Atomic Absorption Spectrometric Determination. *Chem. Eng.* **2019**, *3*, 74.
(13) Kyaw, H. H.; Al-Harthi, S. H.; Sellai, A.; Dutta, J. Self-organization of gold nanoparticles on silanated surfaces. *Beilstein J. Nanotechnol.* **2015**, *6*, 2345−2353.
(14) Baig, N.; Sajid, M.; Saleh, T. A. Recent trends in nanomaterial-modified electrodes for electroanalytical applications. *TrAC, Trends Anal. Chem.* **2019**, *111*, 47−61.
(15) Lo, M.; Diaw, A. K. D.; Gningue-Sall, D.; Aaron, J.-J.; Oturan, M. A.; Chehimi, M. M. Tracking metal ions with polypyrrole thin films adhesively bonded to diazonium-modified flexible ITO electrodes. *Environ. Sci. Pollut. Res.* **2018**, *25*, 20012−20022.
(16) Guo, Z.; Seol, M.-L.; Gao, C.; Kim, M.-S.; Ahn, J.-H.; Choi, Y.-K.; Huang, X.-J. Functionalized porous Si nanowires for selective and simultaneous electrochemical detection of Cd(II) and Pb(II) ions. *Electrochim. Acta* **2016**, *211*, 998−1005.
(17) Bao, Q.; Li, G.; Yang, Z.; Pan, P.; Liu, J.; Chang, J.; Wei, J.; Lin, L. Electrochemical performance of a three-layer electrode based on Bi nanoparticles, multi-walled carbon nanotube composites for simultaneous Hg(II) and Cu(II) detection. *Chin. Chem. Lett.* **2020**, *31*, 2752−2756.
(18) Kim, H.; Kwon, J.-Y. Enzyme immobilization on metal oxide semiconductors exploiting amine functionalized layer. *RSC Adv.* **2017**, *7*, 19656−19661.
(19) Karade, V. C.; Sharma, A.; Dhavale, R. P.; Dhavale, R. P.; Shingte, S. R.; Patil, P. S.; Kim, J. H.; Zahn, D. R. T.; Chougale, A. D.; Salvan, G.; et al. APTES monolayer coverage on self-assembled magnetic nanospheres for controlled release of anticancer drug Nintedanib. *Sci. Rep.* **2021**, *11*, 5674.
(20) Saengdee, P.; Promptmas, C.; Thanapitak, S.; Srisuwan, A.; Pankiew, A.; Thornyanadacha, N.; Chaisriratanakul, W.; Chaowicharat, E.; Jeamsaksiri, W. Optimization of 3-aminopropyl-triethoxysilane functionalization on silicon nitride surface for biomolecule immobilization. *Talanta* **2020**, *207*, No. 120305.
(21) Zhao, P.; Chen, S.; Yang, M.; Wang, Y.; Luo, H.; Huo, D.; Ji, Z.; Hou, C. A novel multifunctional platform based on ITO/APTES/ErGO/AuNPs for long-term cell culture and real-time biomolecule monitoring. *Talanta* **2021**, *228*, No. 122232.
(22) Kaur, A.; Kapoor, S.; Bharti, A.; Rana, S.; Chaudhary, G. R.; Prabhakar, N. Gold-platinum bimetallic nanoparticles coated 3-(aminopropyl)triethoxysilane (APTES) based electrochemical immunosensor for vitamin D estimation. *J. Electroanal. Chem.* **2020**, *873*, No. 114400.
(23) Xiong, Y.; Ma, T.; Zhang, H.; Qiu, L.; Chang, S.; Yang, Y.; Liang, F. Gold nanoparticle functionalized nanopipette sensors for electrochemical paraquat detection. *Microchim. Acta* **2022**, *189*, 251.
(24) Liu, J.; Zhang, H.; Xiaochuan, X.; Aqrab, U. A.; Xue, D.; Huang, H.; Xu, N.; Xi, Q.; Guo, W.; Liang, H. High sensitivity detection of glucose with negatively charged gold nanoparticles functionalized the gate of AlGaN/GaN High Electron Mobility Transistor. *Sens. Actuators, A* **2020**, *312*, No. 112128.
(25) Alruwais, R. S.; Adeosun, W. A.; Marwani, H. M.; Jawaid, M.; Asiri, A. M.; Khan, A. Novel Aminosilane (APTES)-Grafted Polyaniline@Graphene Oxide (PANI-GO) Nanocomposite for Electrochemical Sensor. *Polymers* **2021**, *13*, 2562.
(26) Alruwais, R. S.; Adeosun, W. A.; Alsafrani, A. E.; Marwani, H. M.; Asiri, A. M.; Khan, I.; Jawaid, M.; Khan, A. Development of Cd (II) Ion Probe Based on Novel Polyaniline-Multiwalled Carbon Nanotube-3-aminopropyltriethoxylsilane Composite. *Membranes* **2021**, *11*, 853.
(27) Mohamad Nor, N.; Arivalakan, S.; Zakaria, N. D.; Nilamani, N.; Lockman, Z.; Abdul Razak, K. Self-Assembled Iron Oxide Nanoparticle-Modified APTES-ITO Electrode for Simultaneous Stripping Analysis of Cd(II) and Pb(II) Ions. *ACS Omega* **2022**, *7*, 3823−3833.
(28) Ghazali, N. N.; Mohamad Nor, N.; Abdul Razak, K.; Lockman, Z.; Hattori, T. Hydrothermal synthesis of bismuth nanosheets for modified APTES-functionalized screen-printed carbon electrode in lead and cadmium detection. *J. Nanopart. Res.* **2020**, *22*, 211.
(29) Pudza, M. Y.; Abidin, Z. Z.; Abdul-Rashid, S.; Yasin, F. M.; Noor, A. S. M.; Abdullah, J. Selective and simultaneous detection of cadmium, lead and copper by tapioca-derived carbon dot−modified electrode. *Environ. Sci. Pollut. Res.* **2020**, *27*, 13315−13324.
(30) Lu, Z.; Zhang, J.; Dai, W.; Lin, X.; Ye, J.; Ye, J. A screen-printed carbon electrode modified with a bismuth film and gold nanoparticles for simultaneous stripping voltammetric determination of Zn(II), Pb(II) and Cu(II). *Microchim. Acta* **2017**, *184*, 4731−4740.
(31) Lu, Z.; Dai, W.; Liu, B.; Mo, G.; Zhang, J.; Ye, J.; Ye, J. One pot synthesis of dandelion-like polyaniline coated gold nanoparticles composites for electrochemical sensing applications. *J. Colloid Interface Sci.* **2018**, *525*, 86−96.
(32) Hoo, X. F.; Abdul Razak, K.; Ridhuan, N. S.; Mohamad Nor, N.; Zakaria, N. D. Electrochemical glucose biosensor based on ZnO nanorods modified with gold nanoparticles. *J. Mater. Sci.: Mater. Electron.* **2019**, *30*, 7460−7470.
(33) Ardani, H. K.; Imawan, C.; Handayani, W.; Djuhana, D.; Harmoko, A.; Fauzia, V. Enhancement of the stability of silver nanoparticles synthesized using aqueous extract of Diospyros discolor Willd. leaves using polyvinyl alcohol. *IOP Conf. Ser.: Mater. Sci. Eng.* **2017**, *188*, No. 012056.
(34) Arima, Y.; Iwata, H. Effect of wettability and surface functional groups on protein adsorption and cell adhesion using well-defined mixed self-assembled monolayers. *Biomaterials* **2007**, *28*, 3074−3082.
(35) Al-Gahouari, T.; Sayyad, P.; Ingle, N.; Mahadik, M.; Farea, M.; Mohammed, H.; Shirsat, S.; Shirsat, M. Resolution improvement for anodic stripping signals of lead and detached indium from reduced graphene oxide/indium tin oxide (rGO/ITO) electrode using bromide ion. *Appl. Phys. A: Mater. Sci. Process.* **2021**, *127*, 326.
(36) Anandhakumar, S.; Mathiyarasu, J.; Narasimha Phani, K. L. Anodic stripping voltammetric determination of cadmium using a "mercury free" indium film electrode. *Analyst* **2013**, *138*, 5674−5678.
(37) Liu, T. Z.; Lai, D.; Osterloh, J. D. Indium as Internal Standard in Square Wave Anodic Stripping Analysis of Lead in Blood with Microelectrode Arrays. *Anal. Chem.* **1997**, *69*, 3539−3543.
(38) Salunke, R. S.; Nakate, Y. T.; Umar, A.; Nakate, U. T.; Ahmad, R.; Shirale, D. J. Anodic stripping voltammetry analysis of gold nanoparticles functionalized one-dimensional single polypyrrole nanowire for arsenic sensing. *Surf. Interfaces* **2021**, *23*, No. 100895.
(39) Dutta, S.; Strack, G.; Kurup, P. Gold nanostar electrodes for heavy metal detection. *Sens. Actuators, B* **2019**, *281*, 383−391.
(40) Bagheri Hariri, M.; Siavash Moakhar, R.; Sharifi Abdar, P.; Zargarnezhad, H.; Shone, M.; Rahmani, S. A.; Moradi, N.; Niksefat, V.; Shayar Bahadori, K.; Dolati, A. Facile and ultra-sensitive

https://doi.org/10.1021/acsomega.2c07085
ACS Omega 2023, 8, 16587−16599

voltammetric electrodetection of Hg2+ in aqueous media using electrodeposited AuPtNPs/ITO. *Anal. Methods* **2021**, *13*, 2688−2700.
(41) Bernalte, E.; Arévalo, S.; Pérez-Taborda, J.; Wenk, J.; Estrela, P.; Avila, A.; Di Lorenzo, M. Rapid and on-site simultaneous electrochemical detection of copper, lead and mercury in the Amazon river. *Sens. Actuators, B* **2020**, *307*, No. 127620.

https://doi.org/10.1021/acsomega.2c07085
ACS Omega 2023, 8, 16587−16599